Subwavelength Broadband Perfect Absorption for Unidimensional Open-Duct Problems

Yang Meng, Vicente Romero-García, Gwénaël Gabard, Jean-philippe Groby, Charlie Bricault, Sébastien Goudé

Subwavelength broadband perfect absorption for unidimensional open-duct problems

Yang Meng Vicente Romero-García Gwénaël Gabard Jean-Philippe Groby Charlie Bricault Sébastien Goudé*

Y. Meng, G. Gabard, J.-P. Groby
Laboratoire d'Acoustique de l'Université du Mans (LAUM), UMR CNRS 6613, Institut d'Acoustique - Graduate School (IA-GS), CNRS, Le Mans Université, France.
V. Romero-García
Laboratoire d'Acoustique de l'Université du Mans (LAUM), UMR CNRS 6613, Institut d'Acoustique - Graduate School (IA-GS), CNRS, Le Mans Université, France.
Instituto Universitario de Matemática Pura y Aplicada (IUMPA), Departamento de Matemática Aplicada, Universitat Politècnica de València, Camino de Vera, s/n 46022 València, Spain.
C. Bricault, S. Goudé
Vibrations & Acoustics Laboratory, Valeo Thermal Systems, France.
Email Address: mengyang2116@gmail.com

Keywords: *perfect absorption, absorption bound, open-duct problem, radiation problem*

Passive metamaterials provide efficient solutions for sound absorption in the low-frequency regime with deep subwavelength dimensions. They have been extensively applied in unidimensional reciprocal problems considering that an incident wave is either reflected or transmitted at the outlet boundary. However, the generalized problem with impedance boundary condition is not well understood yet. This work presents a general design methodology of metamaterial absorbers for open-duct problems, which is a special case of impedance outlet boundary encountered in broad practical applications, for example, noise-attenuation problems in heat ventilation and air conditioning (HVAC) systems. By properly using monopolar point scatterers made of arrays of Helmholtz resonators, the design process is significantly simplified: the transfer matrix modelling is sufficiently accurate to describe the acoustic response of the system. A single monopolar point scatterer is insufficient to attenuate both the reflected and radiated waves; a frequency-dependent maximum absorption exists and is derived analytically. To go beyond this absorption bound and achieve perfect absorption, at least two point scatterers are necessary. Specific designs are provided and validated experimentally for maximum or perfect absorption, either at single frequencies or over specific frequency bands.

1 Introduction

Passive metamaterials are either artificial or natural structures benefiting from the mechanism of wave resonances. In acoustics, they have been widely used to realize desired wave phenomena, such as acoustic wave attenuation [1, 2, 3, 4], diffusion [5, 6, 7, 8, 9], one-way transport [11, 12, 13], e.g., acoustic diode [10], tunable high-refractive-index medium [14], subwavelength imaging [15, 16, 17, 18], acoustic cloak [19, 20], acoustic topological insulator [21, 22, 23, 24], etc. Among them, the absorption of airborne sound [25, 26, 27, 28, 29, 30, 31, 32] represents one of the most important applications. Compared with traditional passive acoustic treatments, metamaterials can significantly increase the efficiency in dealing with low-frequency acoustic waves and make subwavelength broadband absorption possible.
In the design process of this type of meta-absorbers, the dispersion properties of the employed metamaterial should be precisely controlled. Among the passive design strategies, the use of coupled resonators, of either monopolar or dipolar types, has been extensively studied (see, for example, [25, 26, 33], Chapter 3 of [34], Chapter 5 of [35], etc.). In the unidimensional (1D) reflection problem (either with a rigid boundary [36, 37, 38] or a soft boundary [39]), perfect absorption can be realized at a given frequency by using a single resonator. In the opposite, the maximum absorption coefficient that can be achieved with either a single monopolar or a dipolar type resonator is $\alpha_{\max} = 1/2$ in the 1D transmission problem [25, 40, 41, 42]; to yield perfect absorption, at least two coupled resonators are necessary, because both types of resonances at the same frequency are required to suppress the reflection and the transmission simultaneously [40, 43]. Note that, by using two resonators of the same type, the distance between them in the wave direction should be properly chosen to produce the other type of resonance [40, 44]. Alternatively, a degenerate resonator [26, 40] could be considered, which is realized by introducing a monopolar and a dipolar resonances at the same position along the wave propagation. The use of degenerate

resonators generally results in spatially compact designs for perfect absorption, at the price of a more difficult design process since the evanescent coupling is usually significant. Notice that the aforementioned strategies are based on the mirror symmetries arising from the boundary of the considered system where the acoustic wave is either totally reflected or totally transmitted [25, 40]. Thus, they can be well applied merely in the reflection and transmission problems. In contrast, the outlet boundary does not preserve mirror symmetries in the 1D open-duct problem, because the corresponding acoustic boundary condition has both resistive and reactive contributions that are frequency dependent. Due to this added complexity, the design strategies of passive absorbers in open-duct systems are not yet well developed, and thus, related applications are still limited.

The general aim of this work is to reveal the absorption behaviors of passive metamaterials in the 1D open-duct problem and to develop corresponding design strategies. To ensure the ventilation in the duct, as well as to simplify the design process, only monopolar resonators loaded to the waveguide are considered. In this scenario, either a single resonator or multiple resonators at the same axial position along the wave direction can be modelled as a point scatterer in the subwavelength regime. By tackling the problem algebraically, it is proved that the absorption coefficient of a single point scatterer cannot exceed a frequency-dependent upper bound $\alpha_{\max}$. General design methodologies are provided to realize $\alpha_{\max}$ either at a single frequency or over a specific frequency band. In a further step, we show how to break this absorption bound toward perfect absorption by employing coupled point scatterers.

2 General methodology of the design

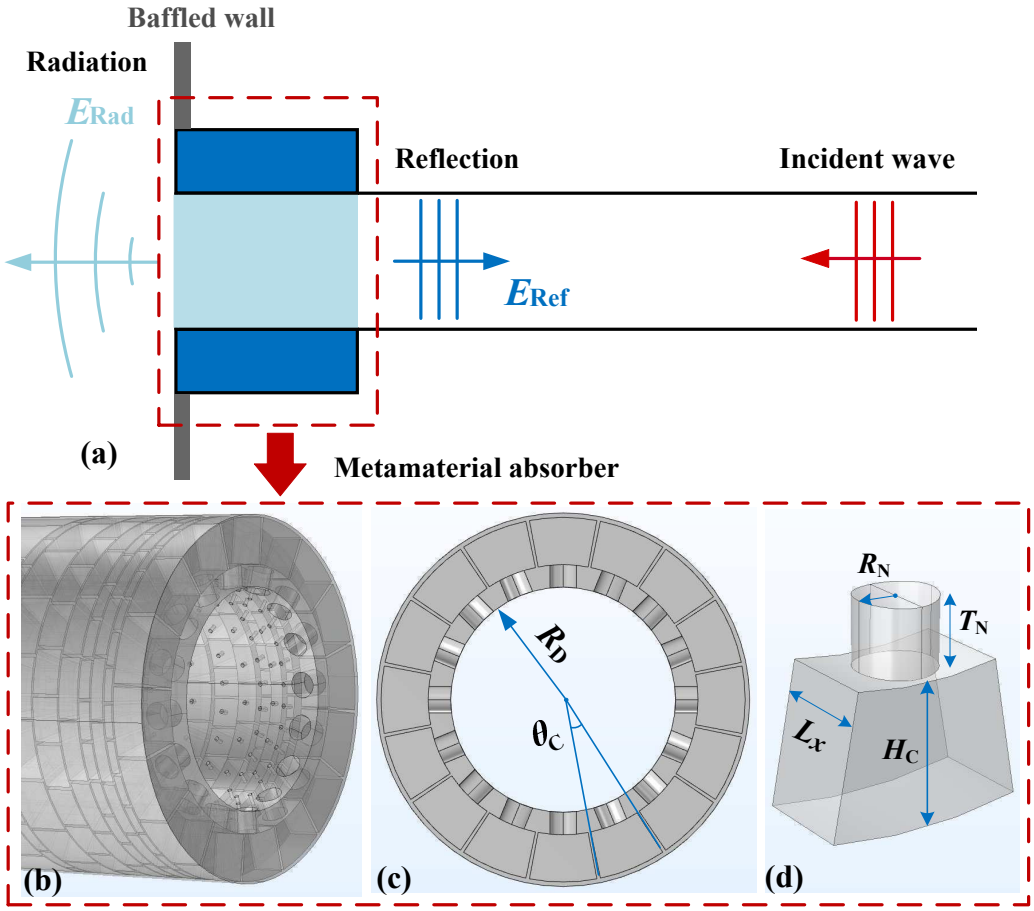

Figure 1: The 1D open-duct problem: the metamaterial absorber realized by monopolar point scatterers is located at the open end of the circular waveguide to reduce both the reflected and radiated wave energy. (a) Schematic illustration of the 1D system. (b) Metamaterial absorber composed of rings of Helmholtz resonators. (c) One monopolar point scatterer made of a single ring of Helmholtz resonators. (d) A single Helmholtz resonator with circular cavity.

The passive metamaterial considered in this work is illustrated in Figure 1 and is made of Helmholtz resonators in both axial and circumferential directions along a circular rigid open duct, whose inner radius is $R_{\mathrm{D}} = 5$ cm (the cut-off frequency is $f = 2010$ Hz). The metamaterial is located near the open end to attenuate both the reflected and radiated waves, i.e., to maximize the absorption coefficient of the system, defined as

$$\alpha = 1 - E_{\mathrm{Ref}} - E_{\mathrm{Rad}}, \tag{1}$$

where E_{Ref} and E_{Rad} are the energies of the reflected and radiated waves normalized by that of the incident wave, respectively. In the low frequency regime, i.e., when the considered frequency band is below the cut-off frequency of the duct, the acoustic performance of the system is dominated by a 1D scattering problem. Then, the above energy coefficients can be written as

$$\begin{cases} E_{\mathrm{Ref}} = \left| \dfrac{p_{\mathrm{Ref}}}{p_{\mathrm{In}}} \right|^2 = |R|^2, \\ E_{\mathrm{Rad}} = z_0 \dfrac{\mathrm{Re}\left(\displaystyle\int_{\Sigma} p^*_{\mathrm{Rad}} \boldsymbol{u}_{\mathrm{Rad}} \cdot \mathrm{d}\boldsymbol{\Sigma} \right)}{|p_{\mathrm{In}}|^2 S_{\mathrm{D}}} = \mathrm{Re}\left(\dfrac{1}{\zeta_{\mathrm{Rad}}} \right) \left| \dfrac{p^+_{\mathrm{Rad}}}{p_{\mathrm{In}}} \right|^2 = \mathrm{Re}\left(\dfrac{1}{\zeta_{\mathrm{Rad}}} \right) |T|^2, \end{cases} \tag{2}$$

where p and $\boldsymbol{u}$ are the acoustic pressure and particle velocity respectively, the subscripts In, Ref, and Rad correspond to the incident, reflected, and radiated waves respectively, $S_{\mathrm{D}} = \pi R_{\mathrm{D}}^2$ is the cross-sectional area of the open duct, the star refers to the complex conjugate, p^+_{Rad} refers to the pressure of the outgoing wave right outside the open end, $z_0 = \rho_0 c_0 = 412$ kg/(m^{2}s) is the characteristic impedance of air, $\rho_0 = 1.2$ kg/m^3 and $c_0 = 343$ m/s are the density and the adiabatic sound speed of air, respectively. Note that E_{Ref} is readily expressed by the pressure reflection coefficient $R = p_{\mathrm{Ref}}/p_{\mathrm{In}}$, whereas the radiated wave energy E_{Rad} (or equivalently the sound power) is derived from the integration of sound intensity on the outer-field surface Σ. Specifically, when Σ is chosen as that of the open end of the duct, E_{Rad} can be expressed with the pressure transmission coefficient $T = p^+_{\mathrm{Rad}}/p_{\mathrm{In}}$ and the specific radiation impedance ζ_{Rad} of the open end. Following the $\mathrm{e}^{\mathrm{i}\omega t}$ convention ($\omega = 2\pi f$ is the angular frequency), ζ_{Rad} for a baffled circular open duct can be explicitly written as (see, for example, page 186 of [45])

$$\zeta_{\mathrm{Rad}} = \left[\frac{p}{z_0 u} \right]_{\text{Open end}} = 1 - \frac{J_1(2k_0 R_{\mathrm{D}})}{k_0 R_{\mathrm{D}}} + \mathrm{i} \frac{SH_1(2k_0 R_{\mathrm{D}})}{k_0 R_{\mathrm{D}}}, \tag{3}$$

where J_1 is the first-order Bessel function of the first kind, SH_1 denotes the first-order Struve-H function, and $k_0 = \omega/c_0$ is the acoustic wavenumber. By using the transfer matrix method [34, 35], the reflection and transmission coefficients R and T in Equations (2) and thus the absorption coefficient α in Equation (1) can be explicitly expressed as functions of the radiation impedance ζ_{Rad} (i.e. a known function of frequency) as well as the structural parameters of the Helmholtz resonators. Specifically, the acoustic response of each resonator is fully determined by 6 structural parameters: the radius R_{N} and thickness T_{N} of the neck, the depth H_{C}, axial width L_x, and circular angle θ_{C} of the cavity, as well as the axial position x_{HR} of the resonator (see Figure 1). Then, the absorption coefficient can be expressed as

$$\alpha = \alpha(f; R_{\mathrm{N},i}, T_{\mathrm{N},i}, H_{\mathrm{C},i}, L_{x,i}, \theta_{\mathrm{C},i}, x_{\mathrm{HR},i}), \ \ i = 1, 2, 3, ..., N_{\mathrm{HR}}, \tag{4}$$

where N_{HR} denotes the total number of resonators. Notice that, these $6 \times N_{\mathrm{HR}}$ geometric variables are not fully independent with each other for the designs considered in this work. For instance, we assume that the resonators employed within one ring have identical axial length L_x. The closed-form expression of α and details of the transfer-matrix modelling of α as well as the other aforementioned coefficients (R, T, E_{Ref}, and E_{Rad}) are provided in the supporting material. With the theoretical expression of α, the geometric optimizations can be carried out to design absorbers working either at a single frequency f_1 or over a frequency band from f_1 to f_2, by using the cost functions

$$\max_{f=f_1} [\alpha(f)], \quad \text{or} \quad \max \left[\frac{\int_{f_1}^{f_2} \alpha(f) \mathrm{d}f}{f_2 - f_1} \right], \tag{5}$$

respectively. The constrained nonlinear minimization method [46] implemented in the Matlab® function *fmincon* is then applied to tune the geometric parameters, so that the optimized solution of the problem, i.e., the optimized design, can be acquired. Note that, in all the cases studied in this work, several local extrema can be found, which achieve similar absorption spectra. In practice, the designs which are robust to the truncation errors of the dimensions (i.e. the geometric parameters) are chosen, considering that the accuracy of 3D printing which we apply is fixed at 0.1 mm.

3 Monopolar point-scatterer metamaterial: absorption bound and broadband maximum absorption in open-duct problems

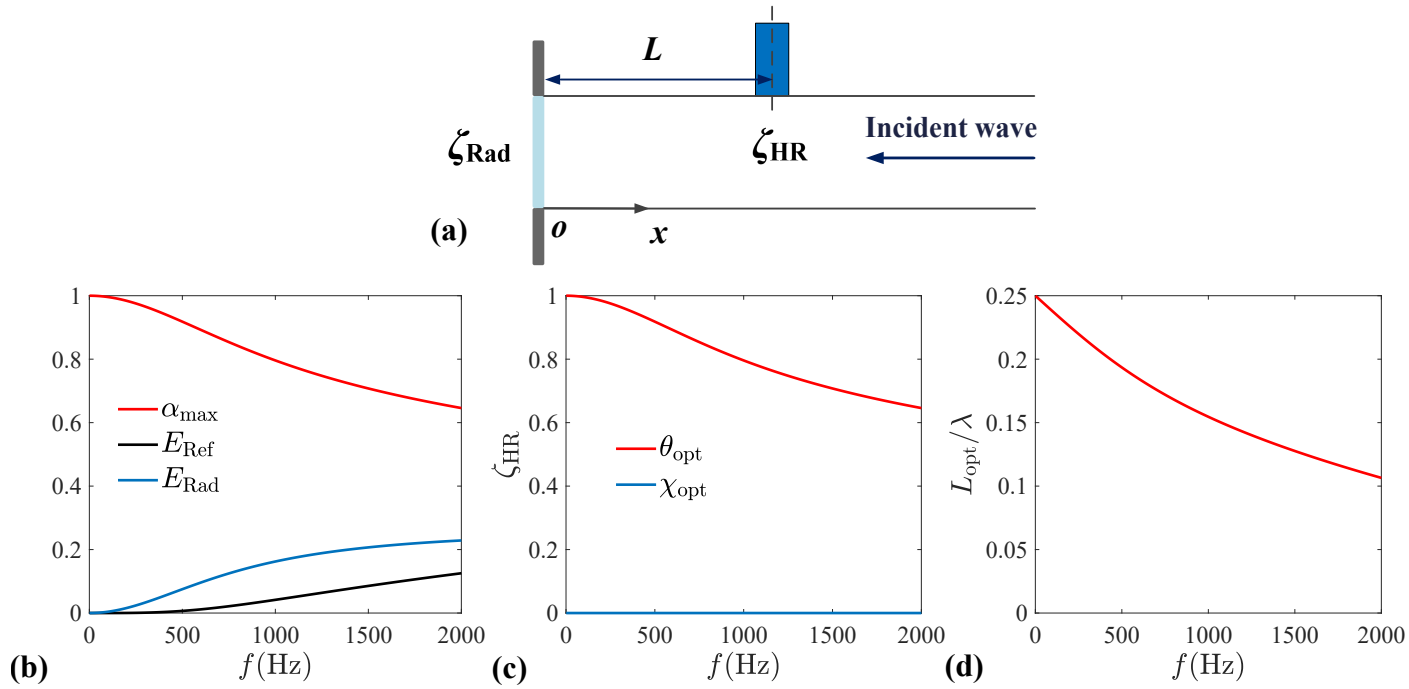

Figure 2: The absorption bound of a monopolar point scatterer: (a) Schematic illustration of the point-scatterer metamaterial in the 1D open-duct problem. (b) Absorption bound. (c) Optimal impedance for the maximum absorption coefficient. (d) Optimal position for the maximum absorption coefficient.

Firstly, we consider the acoustic performance of a monopolar point scatterer in the circular waveguide with $R_{\mathrm{D}} = 5$ cm. In Figure 2(a), the point scatterer located at $x = L$ in the 1D open-duct system refers to a single ring of Helmholtz resonators distributed along the circumferential direction. In this situation, perfect absorption is unachievable; the upper bound on the absorption coefficient is derived as (see the supporting material)

$$\alpha_{\max} = \frac{1}{2}\left\{1 + \sqrt{\frac{J_1^2(\kappa) + SH_1^2(\kappa)}{[J_1(\kappa) - \kappa]^2 + SH_1^2(\kappa)}}\right\}, \tag{6}$$

where $\kappa = 2k_0R_{\mathrm{D}}$ is the Helmholtz number defined with the diameter of the open duct. Equation (6) indicates that $\alpha_{\max}$ is a monotonically decreasing function of frequency, as shown in Figure 2(b). In the static limit (i.e. $f \to 0$), $\alpha_{\max}$ tends to unity, since perfect absorption is achievable in the reflection problem (note: the open end reduces to a pressure-release boundary, i.e. $\zeta_{\mathrm{Rad}} \to 0$, when $f \to 0$). In the opposite, the open end becomes less reflective when frequency increases. As a consequence, $\alpha_{\max}$ decreases with frequency and approaches 1/2 in the dynamic limit (i.e. $f \to \infty$), when the open end is not reflecting at all and the system reduces to a 1D transmission problem. Note that the dynamic limit here is merely a mathematical limit in the 1D problem, since higher order modes may exist in the waveguide in the real physical system and the 1D model becomes inaccurate.

In order to achieve $\alpha_{\max}$ at any frequency, both the axial position (L) and the surface impedance (ζ_{HR}) of the point scatterer should be properly chosen. The surface impedance is defined by $\zeta_{\mathrm{HR}} = \theta + \mathrm{i}\chi = p/(z_0 Q)$, where θ and χ refer to the resistance and reactance respectively, $Q = uS_{\mathrm{N}}/S_{\mathrm{D}}$ is the volume flux, S_{D} and S_{N} are the areas of the waveguide cross section and neck(s) of the Helmholtz resonator(s), respectively. From Figure 2(c) the optimal impedance ($\zeta_{\mathrm{opt}} = \theta_{\mathrm{opt}} + \mathrm{i}\chi_{\mathrm{opt}}$) is purely resistive. In addition, a series of frequency-dependent positions $x = L_{\mathrm{opt}}(n) \equiv L_{\mathrm{opt}}(0) + n\lambda$ should be chosen to achieve $\alpha_{\max}$, where $n = 0, 1, 2, ...$ and $\lambda = 2\pi/k_0$ is the considered wavelength. In Figure 2(d), the particular optimal distance $L_{\mathrm{opt}}(0)$ (nearest to the open end) is plotted, which indicates that L_{opt} decreases with frequency. Particularly, L_{opt} approaches the quarter wavelength in the static limit. However, this is not physically achievable in principle, since the wavelength tends to infinity in that limit. The explicit expressions of ζ_{opt} and $L_{\mathrm{opt}}(n)$ are provided in the supporting material.

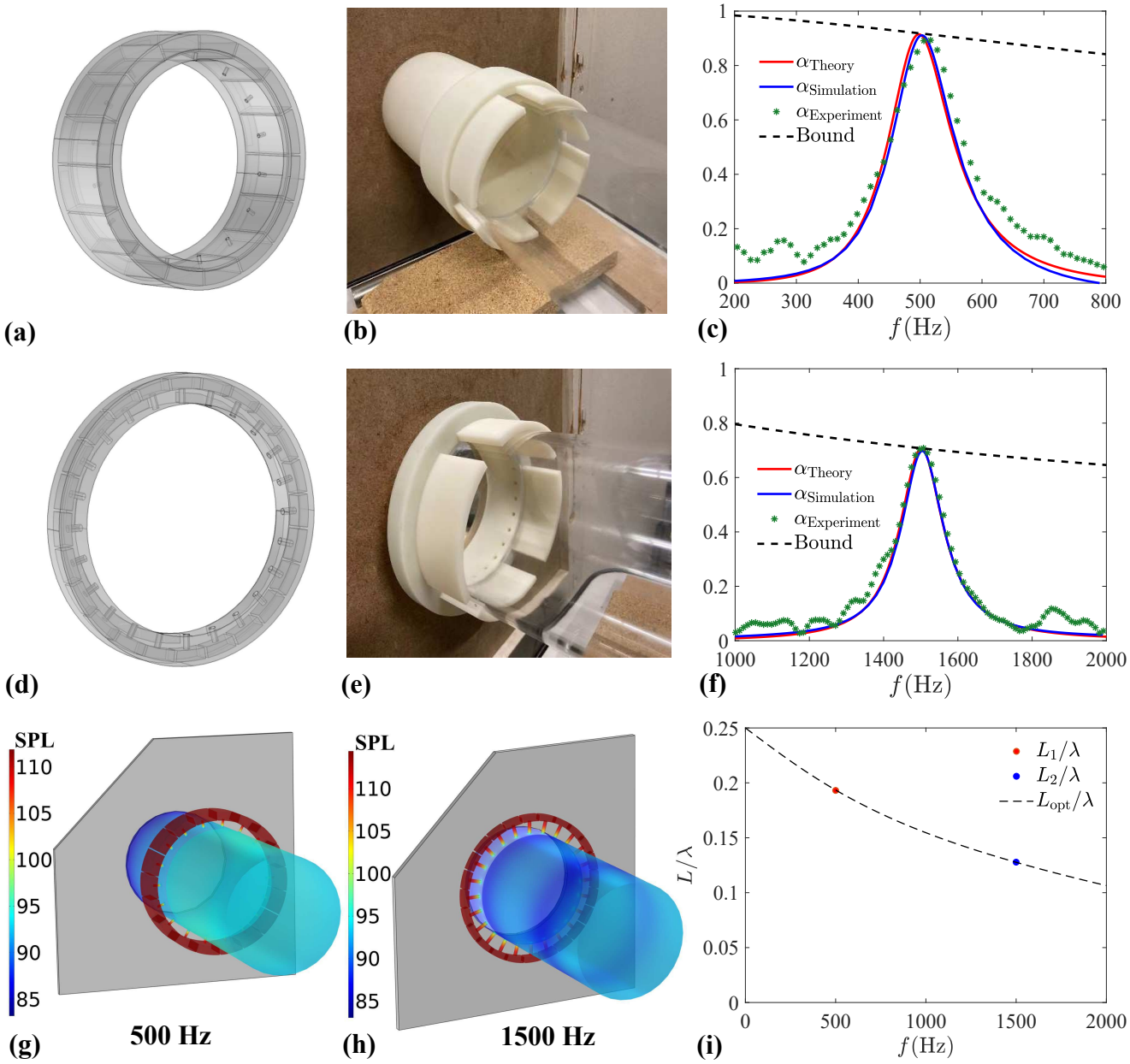

Figure 3: Designs of monopolar point scatterers for maximum absorption at single frequency: (a) Sample 1 working at 500 Hz made of 16 identical Helmholtz resonators. (b) Sample 1 under test. (c) Absorption coefficient of Sample 1: comparison of the theoretical result, numerical simulation, and the experimental measurement. (d) Sample 2 working at 1500 Hz made of 24 identical Helmholtz resonators. (e) Sample 2 under test. (f) Absorption coefficient of Sample 2: comparison of the theoretical result, numerical simulation, and experimental measurement. (g) The simulated SPL distribution of Sample 1 with 500 Hz incident wave (from the right to the left). (h) The simulated SPL distribution of Sample 2 with 1500 Hz incident wave (from the right to the left). (i) The optimal axial positions of the point scatterers as functions of frequency.

By applying the optimization method, two specific point scatterers are designed for maximum absorption at 500 Hz and 1500 Hz. In these designs, 16 and 24 identical resonators are used respectively, which are arranged in a single ring. Note that 16 and 24 are fixed input values. Then, the design method provides optimized structural parameters of the resonators. The design theory is validated against both numerical simulations and experimental measurements provided in Figures 3(c) and (f). The simulated sound-pressure-level (SPL) distributions of the samples at their absorption peak frequencies (500 Hz and 1500 Hz) are shown in Figures 3(g) and (h), respectively (Note: in all the simulations of this work, the incident wave has the pressure amplitude of 1 Pa, which is approximately 94 dB in SPL). The SPL inside the resonators are considerably higher than that in the waveguide, because these resonators are work-

ing at their resonant frequencies (the optimal impedance has vanishing reactive parts). Besides, the axial distances between the outlet and the point scatterer are 0.1931λ and 0.1278λ respectively, which are well predicted by the theory as shown in Figure 3(i).

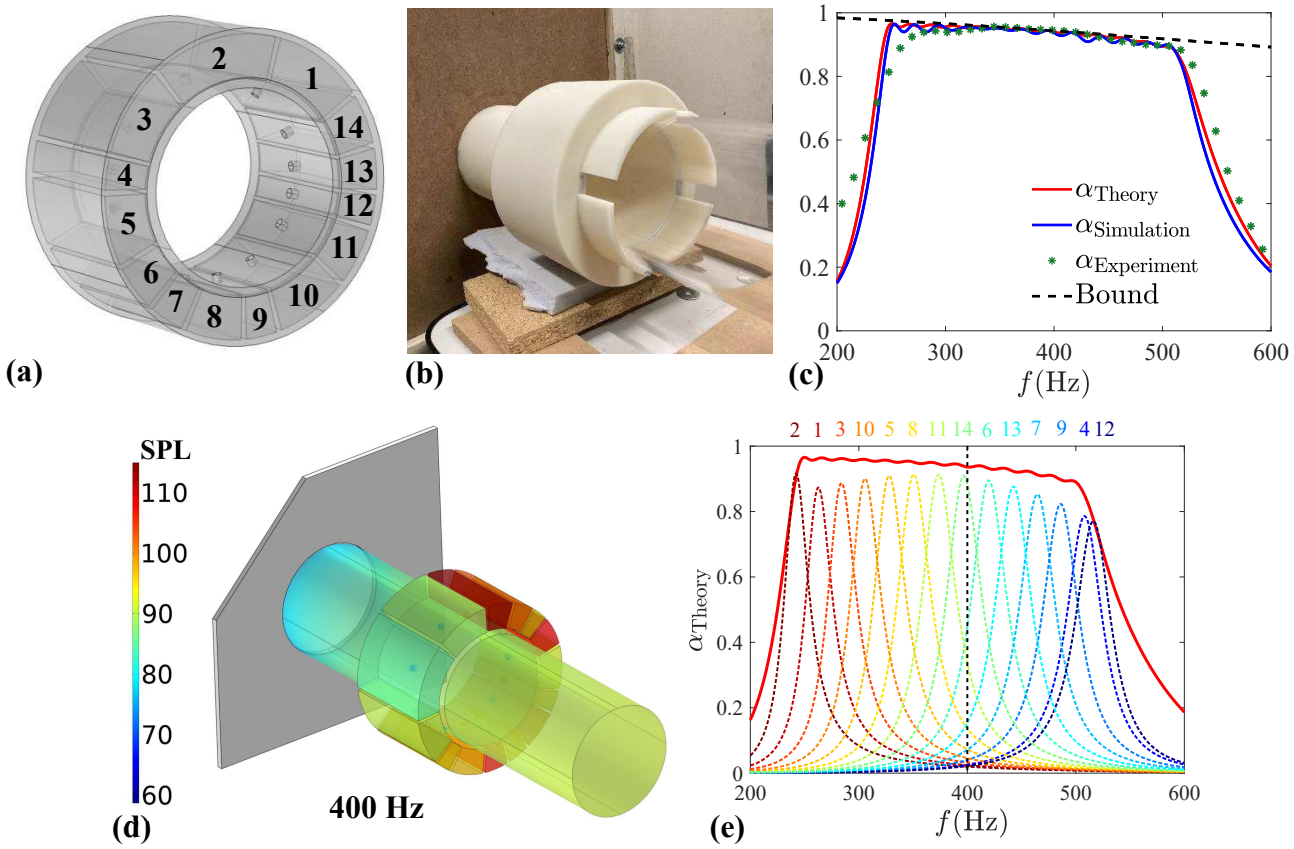

Figure 4: Design of monopolar point-scatterer metamaterial for broadband maximum absorption with deep subwavelength size: (a) Sample working from 250 Hz to 500 Hz made of 14 different Helmholtz resonators. (b) Sample under test. (c) Absorption coefficient of the sample: comparison of the theoretical result, numerical simulation, and experimental measurement. (d) The simulated SPL distribution of the sample with 400 Hz incident wave (from the right to the left). (e) Theoretical absorption coefficients of the 14 individual resonators and that of the whole sample (the thick red curve above).

According to Figure 3(b), $\alpha_{\max} > 0.9$ when $f < 500$ Hz. Thus, it is possible to design efficient broadband absorber in the low frequency range by introducing more degrees of freedom, i.e., using multiple resonators. This idea is realized by the sample shown in Figures 4(a) and 4(b), where 14 detuned Helmholtz resonators are used along the circumferential direction to achieve maximum absorption within the octave from 250 Hz to 500 Hz. Note that all the resonators have identical axial length (L_x) and radial height ($T_{\text{N}} + H_{\text{C}}$). The axial distance from the outlet to the centre of the necks is $L = 0.177$ m, which is the optimal position for $f = 397$ Hz (i.e., $L/\lambda_{397\text{Hz}} = 0.2039$ is on the curve predicted by Figure 2(d)). Thus, $\alpha_{\max}$ can be reached only at this single frequency. However, as demonstrated by the results shown in Figure 4(c), the design value can be controlled close to $\alpha_{\max}$ in the considered octave. According to the experiment, more than 90% of the incident energy within 250 Hz to 500 Hz is absorbed corresponding to the physical bound, whereas the total length of the absorber (including the length of the scatterer as well as the distance to the open end) is merely 19% of the wavelength at 250 Hz. The simulated SPL distribution within the absorber at 400 Hz is provided in Figure 4(d). The 14th resonator has an absorption peak near 400 Hz and thus has considerably high SPL within the cavity. Besides, the absorption performances of individual resonators are shown in Figure 4(e). The absorption peaks of all the individuals are distributed in the considered frequency band with almost identical Δf, whereas the peaks are slightly below the absorption curve achieved by the whole sample (the thick red curve in the figure), which indicates that the impedances of the resonators are close to the optimal values for $\alpha_{\max}$ at these frequencies, or equivalently, the individuals are weakly coupled to achieve the broadband $\alpha_{\max}$.

4 Coupled point-scatterer metamaterial: broadband perfect absorption in the open-duct problem

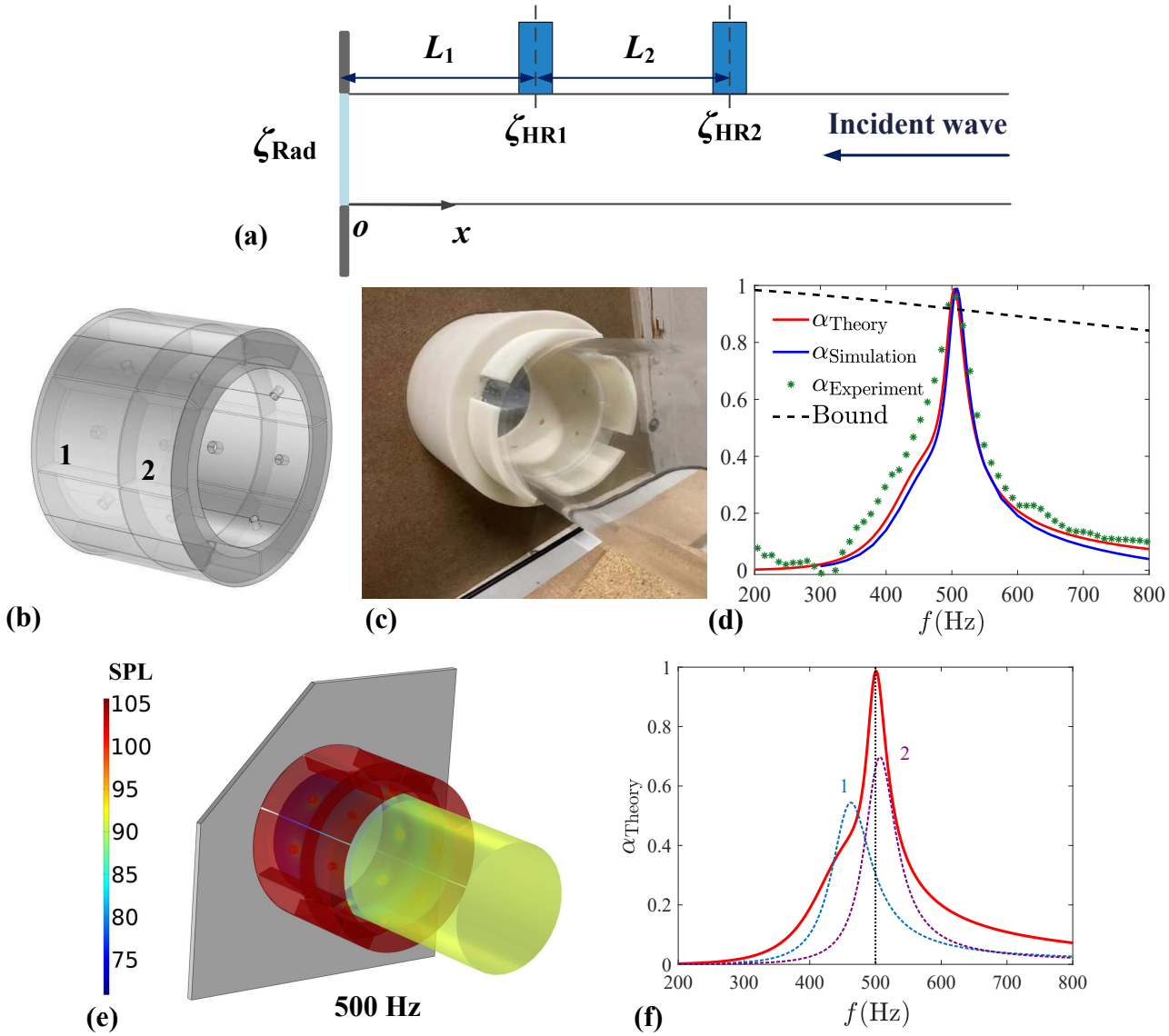

Figure 5: Design of coupled point-scatterer metamaterial for perfect absorption at a single frequency: (a) Schematic illustration of two coupled point scatterers in the open-duct problem. (b) Sample for perfect absorption at 500 Hz made of 2 rings (8+8) of Helmholtz resonators. (c) Sample under test. (d) Absorption coefficient of the sample: comparison of the theoretical result, numerical simulation, and experimental measurement. (e) The simulated SPL distribution of the sample with 500 Hz incident wave (from the right to the left). (f) Theoretical absorption coefficients of the two individual ring scatterers and that of the whole sample (the thick red curve).

In the open-duct problem, the outlet boundary condition is both resistive and reactive, as shown in Equation (3). Consequently, the boundary of the system loses the mirror symmetries present in the 1D reflection and the 1D transmission problems [25, 40, 43]. Thus, at least two detuned point scatterers separated by an axial distance L_2 (as shown in Figure 5(a)) are required to break the absorption bound in Equation (6) and to achieve perfect absorption. Specifically, the impedance of the two scatterers must satisfy

$$\begin{cases} \zeta_{\mathrm{HR1}} = 0 \ , \\ \zeta_{\mathrm{HR2}} = -\mathrm{i}\sin(k_0 L_2)\mathrm{e}^{\mathrm{i}k_0 L_2} \ . \end{cases} \tag{7}$$

Equation (7) indicates that the scatterer HR1 should be working at its resonance frequency (i.e., the incident wave is totally reflected back). Because any incident wave at the outlet could result in a specific

amount of radiation energy, perfect absorption can be achieved only if the incident wave does not reach the outlet. Moreover, when HR1 produces this total reflection boundary (i.e., pressure release boundary), the distance L_1 as well as the outlet boundary condition ζ_{Rad} do not affect the acoustical response of the system any longer. Meanwhile, the other scatterer HR2 works in a reflection problem at this particular frequency, and thus, HR2 can be tuned for perfect absorption with any given distance L_2.
In realistic physical systems, viscothermal losses cannot be avoided. Therefore, perfect absorption at any single frequency is not physically accessible in principle. However, ζ_{HR1} can be tuned as close to zero as possible in practice through proper design strategies, e.g., by increasing the open area ratio of the resonators, etc. As a consequence, perfect absorption can be well approximated. Besides, according to Equation (7), neither HR1 nor HR2 should achieve the optimal impedance for $\alpha_{\max}$ of a single point scatterer. This implies that the scatterers could have considerably low absorption coefficient (compared to $\alpha_{\max}$) at the target frequency. And thus, to achieve perfect absorption, the individual point scatterers should be strongly coupled, in contrast to the previous case with 14 weakly coupled resonators in a single scatterer. Notice that, compared to either the aforementioned strong or weak coupling effects, the evanescent coupling can be neglected.
A design employing two coupled scatterers (each of them is made of 8 identical resonators illustrated in Figure 5(b)) is carried out for perfect absorption at 500 Hz. The distance between the two scatterers is half the total axial width of the absorber, which is $L_2 = 4.9$ cm. Due to Equation (7), the optimal impedances are readily predicted by $\zeta_{\mathrm{HR1}} = 0 + 0\mathrm{i}$ and $\zeta_{\mathrm{HR2}} = 0.19 - 0.39\mathrm{i}$. In contrast, the two ring scatterers in the optimized design have the theoretical impedances $\zeta_{\mathrm{Ring1}} = 0.097 + 0.0016\mathrm{i}$ and $\zeta_{\mathrm{Ring2}} = 0.18 - 0.48\mathrm{i}$ respectively, which are in good agreement with the predictions of $\zeta_{\mathrm{HR1,2}}$. The corresponding geometric parameters of this design are provided in the supporting material. The design theory is further validated by simulations and measurements, as shown in Figure 5(d). The simulated SPL distribution of the sample at 500 Hz are given in Figure 5(e). Besides, the absorption performances of each single ring scatterer separately are shown in Figure 5(f). The absorption coefficient of either Ring 1 or Ring 2 is below 0.65 at 500 Hz, which is considerably lower than $\alpha_{\max}$ (~ 0.9). However, due to their coupling effect, this design provides nearly perfect absorption at the target frequency. Specifically, according to the measurement, more than 95% of the incident wave energy is absorbed within the narrow band between 495 Hz and 505 Hz.

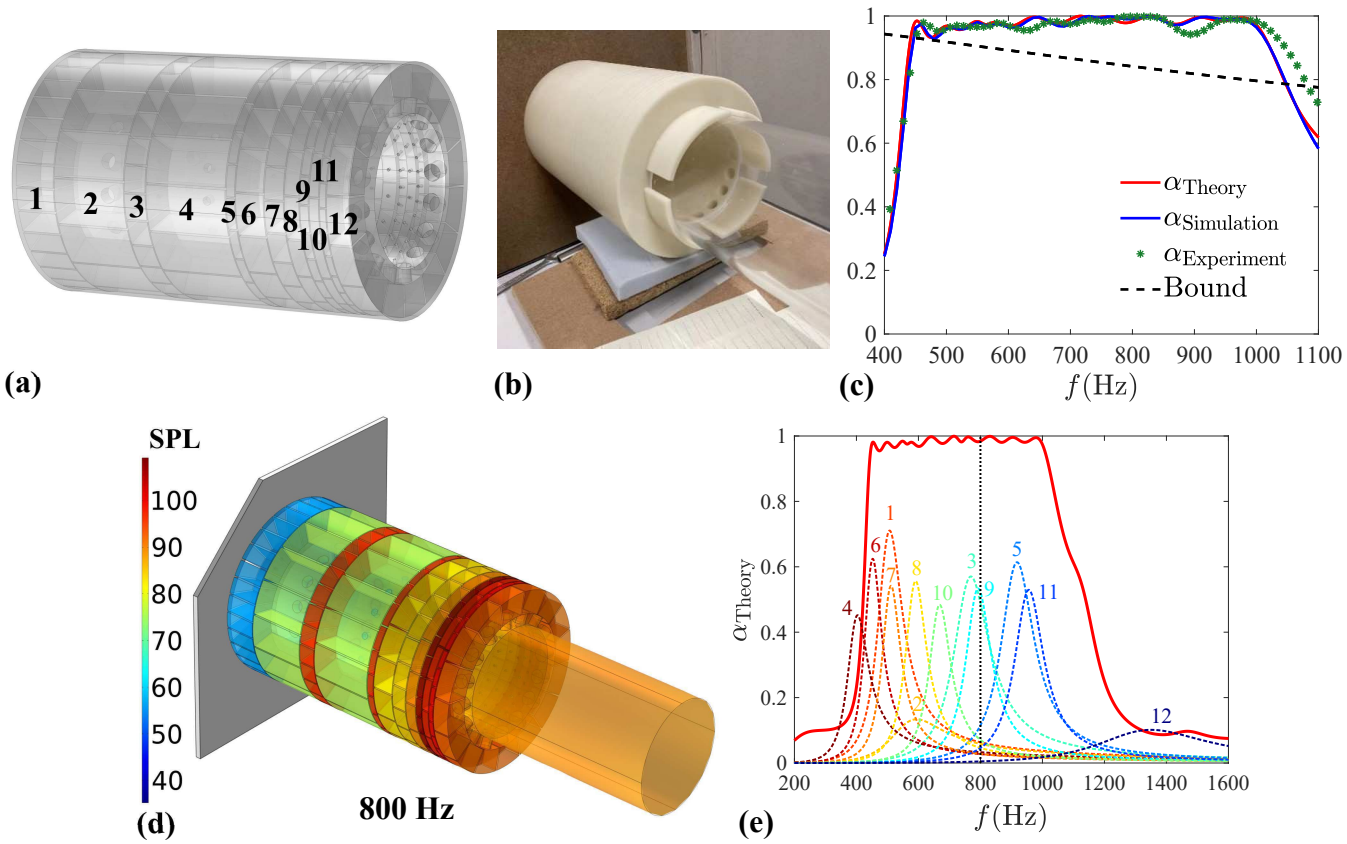

Figure 6: Design of coupled point-scatterer metamaterial for broadband perfect absorption: (a) Sample for perfect absorption from 450 Hz to 1000 Hz made of 12 rings of Helmholtz resonators. (b) Sample under test. (c) Absorption coefficient of the sample: comparison of the theoretical result, numerical simulation, and experimental measurement. (d) The simulated SPL distribution of the sample with 800 Hz incident wave (from the right to the left). (e) Theoretical absorption coefficients of 12 individual ring scatterers and that of the whole sample (the thick red curve above).

The idea of using coupled point scatterers for perfect absorption at a single frequency can be readily generalized for the design of broadband absorbers. A specific design for perfect absorption from 450 Hz to 1000 Hz is carried out, in which 12 point scatterers (comprising 16 to 32 identical resonators in each ring) are employed, as illustrated in Figure 6(a). The total length of the absorber is 25 cm and the radial thickness of the ring-shaped scatterers is 3.2 cm. Validations of the design are presented in Figure 6(c). The simulated SPL distribution of the sample at 800 Hz is shown in Figure 6(d). Besides, the theoretical predictions on the absorption coefficients produced by individual rings are provided in Figure 6(e). It can be found that the absorption peaks of the 12 individuals are below 0.7, and moreover, the peaks of Ring 4 and Ring 12 are outside the considered frequency band. However, broadband perfect absorption can be achieved approximately by utilizing these strongly coupled point scatterers. According to the measurement, more than 97% of the incident wave energy is absorbed between 450 Hz to 1000 Hz.

5 Conclusion

The absorption of both reflected and radiated acoustic waves by using monopolar point scatterers in open-duct problems is studied in this work. With a single point scatterer, the maximum absorption coefficient ($\alpha_{\max}$) is frequency dependent and less than unity in general. To achieve $\alpha_{\max}$ at a single frequency, two conditions are necessary: a) the scatterer provides the optimal impedance ζ_{opt} and b) the distance between the scatterer and the open end is the optimal value L_{opt}. In contrast, to achieve perfect absorption ($\alpha = 1$), at least two point scatterers are needed. Moreover, it is required that: a) the scatterer near the open end has infinitesimal impedance and b) the other scatterer has specific optimal impedance (Equation (7)), which depends merely on the distance between the two scatterers.

To realize $\alpha_{\max}$ and also perfect absorption, either at a single frequency or over a specific frequency band, we propose a general design strategy, in which monopolar point scatterers are employed. These point scatterers are made of arrays of Helmholtz resonators in parallel with the open duct, i.e., in both the circumferential and the wave directions. The theoretical prediction on the absorption bound ($\alpha_{\max}$) of a single point scatterer is then validated by specific designs (at 500 Hz and 1500 Hz, respectively). Moreover, the prediction indicates that $\alpha_{\max}$ is close to perfect in the low frequency range, i.e., for a circular tube with $R_{\mathrm{D}} = 5$ cm considered in this work, $\alpha_{\max} \geq 0.9$ for $f \leq 500$ Hz. Thus, a compact and efficient absorber is realized by utilizing this property with a single point scatterer made of detuned Helmholtz resonators, which possesses deep subwavelength size and achieves broadband (250 Hz to 500 Hz) maximum absorption. In contrast, coupled point scatterers are necessary to break the absorption bound and thus to achieve perfect absorption. Specific designs are provided for perfect absorption either at a single frequency (500 Hz) or over a specific frequency band slightly larger than one octave (450 Hz to 1000 Hz). All the designs in this work are validated with theoretical, numerical and experimental demonstrations. The design strategy will find promising physical and engineering applications and are readily generalized, for example, to consider a different waveguide geometry or to include the effect of an arbitrarily provided passive impedance boundary condition at the end of the waveguide, etc.

6 Experimental Section

3D Printed Samples: The designed metamaterial samples were 3D printed with photosensitive resins using selective laser sintering (SLS) 3D printing method. The printing accuracy was 0.1 mm and all the samples had smooth surfaces which did not introduce additional viscothermal losses to the systems. All the samples were purchased from Centre de Transfert de Technologie du Mans (CTTM)*.

Experimental measurement of the absorption coefficient: All the experimental measurements were carried out in the anechoic room of Laboratoire d'Acoustique de l'Université du Mans (LAUM). In the measurements, the samples were installed at the end of a polyvinyl chloride (PVC) tube with inner radius 5 cm and total length 2 m. A 1.5 m $\times$ 2 m rigid plate was employed as the baffled wall. The standard two-microphone method [47] was used to measure the incident and reflected wave energies inside the PVC tube. Meanwhile, the acoustic pressure in the outer field (1 m^2 region) was measured with a scanning robot; the radiation energy could be derived from the measured pressure field. Then, the absorption coefficient was obtained with Equations (1) and (2). More details of the setups and validations are provided in the supporting material.

Numerical simulation: The pressure acoustics, frequency domain interface of COMSOL Multiphysics® was used to simulate the acoustic performances of the samples. The plane incident wave was driven by a background pressure field (whose axial length is 5 cm) within the circular duct on the upstream side of the absorber. Perfect matched layers (PMLs) were introduced to suppress reflected waves at both the upstream end of the duct and the boundary of the outer field (which is a semi-sphere with the radius of 1 m). The viscothermal losses were accounted for by imposing the thermoviscous boundary layer impedance condition at all the rigid walls. The absorption coefficients were then calculated from the simulated pressure field using the same method as that in the experiments.

Supporting Information
Supporting Information is available from the Wiley Online Library or from the author.

Acknowledgements
All the authors gratefully acknowledge the support of Valeo. J.-P. G. and V. R.-G. would like to acknowledge the support of the ANR-RGC METARoom project (ANR-18-CE08-0021).

*CTTM website: http://www.cttm-lemans.com/fr/index.html

References

[1] M. Yang, P. Sheng, *Annual Review of Materials Research* **2017**, *47* 83.

[2] S.-H. Seo, Y.-H. Kim, K.-J. Kim, *Applied Acoustics* **2018**, *138* 188.

[3] R. Ghaffarivardavagh, J. Nikolajczyk, S. Anderson, X. Zhang, *Physical Review B* **2019**, *99*, 2 024302.

[4] L. Wu, Z. Zhai, X. Zhao, X. Tian, D. Li, Q. Wang, H. Jiang, *Advanced Functional Materials* **2022**, *32*, 13 2105712.

[5] B. Xie, K. Tang, H. Cheng, Z. Liu, S. Chen, J. Tian, *Advanced Materials* **2017**, *29*, 6 1603507.

[6] N. Jiménez, T. J. Cox, V. Romero-García, J.-P. Groby, *Scientific reports* **2017**, *7*, 1 1.

[7] Z. Tian, C. Shen, J. Li, E. Reit, Y. Gu, H. Fu, S. A. Cummer, T. J. Huang, *Advanced Functional Materials* **2019**, *29*, 13 1808489.

[8] E. Ballestero, N. Jimenez, J.-P. Groby, H. Aygun, S. Dance, V. Romero-García, *Applied Physics Letters* **2021**, *119*, 4 044101.

[9] N. Jiménez, J.-P. Groby, V. Romero-García, *Scientific reports* **2021**, *11*, 1 1.

[10] B. Liang, B. Yuan, J. Cheng, *Phys. Rev. Lett.* **2009**, *103* 104301.

[11] X. Zhu, X. Zou, B. Liang, J. Cheng, *Journal of Applied Physics* **2010**, *108*, 12 124909.

[12] C. He, X. Ni, H. Ge, X.-C. Sun, Y.-B. Chen, M.-H. Lu, X.-P. Liu, Y.-F. Chen, *Nature physics* **2016**, *12*, 12 1124.

[13] A. Darabi, L. Fang, A. Mojahed, M. D. Fronk, A. F. Vakakis, M. J. Leamy, *Phys. Rev. B* **2019**, *99* 214305.

[14] X. Zhu, K. Li, P. Zhang, J. Zhu, J. Zhang, C. Tian, S. Liu, *Nature Communications* **2016**, *7*, 1 1.

[15] J. Zhu, J. Christensen, J. Jung, L. Martin-Moreno, X. Yin, L. Fok, X. Zhang, F. Garcia-Vidal, *Nature physics* **2011**, *7*, 1 52.

[16] C. Ma, S. Kim, N. X. Fang, *Nature communications* **2019**, *10*, 1 1.

[17] Y.-X. Shen, Y.-G. Peng, F. Cai, K. Huang, D.-G. Zhao, C.-W. Qiu, H. Zheng, X.-F. Zhu, *Nature communications* **2019**, *10*, 1 1.

[18] L.-S. Zeng, Z.-M. Li, Z.-B. Lin, H. Wu, Y.-G. Peng, X.-F. Zhu, *Applied Physics Letters* **2022**, *120*, 20 202202.

[19] Y. Cheng, F. Yang, J. Y. Xu, X. J. Liu, *Applied Physics Letters* **2008**, *92*, 15 151913.

[20] S. Zhang, C. Xia, N. Fang, *Physical review letters* **2011**, *106*, 2 024301.

[21] Y.-G. Peng, C.-Z. Qin, D.-G. Zhao, Y.-X. Shen, X.-Y. Xu, M. Bao, H. Jia, X.-F. Zhu, *Nature communications* **2016**, *7*, 1 1.

[22] Z. Zhang, Y. Tian, Y. Wang, S. Gao, Y. Cheng, X. Liu, J. Christensen, *Advanced Materials* **2018**, *30*, 36 1803229.

[23] Z. Zhang, H. Long, C. Liu, C. Shao, Y. Cheng, X. Liu, J. Christensen, *Advanced Materials* **2019**, *31*, 49 1904682.

[24] Y. Ding, Y. Peng, Y. Zhu, X. Fan, J. Yang, B. Liang, X. Zhu, X. Wan, J. Cheng, *Phys. Rev. Lett.* **2019**, *122* 014302.

[25] A. Merkel, G. Theocharis, O. Richoux, V. Romero-García, V. Pagneux, *Applied Physics Letters* **2015**, *107*, 24 244102.

[26] M. Yang, C. Meng, C. Fu, Y. Li, Z. Yang, P. Sheng, *Applied Physics Letters* **2015**, *107*, 10 104104.

[27] M. Yang, S. Chen, C. Fu, P. Sheng, *Materials Horizons* **2017**, *4*, 4 673.

[28] N. Jiménez, V. Romero-García, V. Pagneux, J.-P. Groby, *Phys. Rev. B* **2017**, *95* 014205.

[29] L.-j. Li, B. Zheng, L.-m. Zhong, J. Yang, B. Liang, J.-c. Cheng, *Applied Physics Letters* **2018**, *113*, 10 103501.

[30] T. Lee, T. Nomura, H. Iizuka, *Scientific reports* **2019**, *9*, 1 1.

[31] T. Lee, T. Nomura, E. M. Dede, H. Iizuka, *Phys. Rev. Appl.* **2019**, *11* 024022.

[32] X. Xiang, X. Wu, X. Li, P. Wu, H. He, Q. Mu, S. Wang, Y. Huang, W. Wen, *Extreme Mechanics Letters* **2020**, *39* 100786.

[33] V. Romero-García, G. Theocharis, O. Richoux, A. Merkel, V. Tournat, V. Pagneux, *Scientific reports* **2016**, *6*, 1 1.

[34] V. Romero-Garcia, A.-C. Hladky-Hennion, editors, *Fundamentals and applications of acoustic metamaterials: From seismic to radio frequency*, John Wiley & Sons, **2019**.

[35] N. Jiménez, O. Umnova, J.-P. Groby, editors, *Acoustic waves in periodic structures, metamaterials, and porous media: From fundamentals to industrial applications*, Springer, Cham, **2021**.

[36] S. Huang, X. Fang, X. Wang, B. Assouar, Q. Cheng, Y. Li, *The Journal of the Acoustical Society of America* **2019**, *145*, 1 254.

[37] S. Huang, Z. Zhou, D. Li, T. Liu, X. Wang, J. Zhu, Y. Li, *Science Bulletin* **2020**, *65*, 5 373.

[38] S. Qu, P. Sheng, *Physical Review Applied* **2022**, *17*, 4 047001.

[39] H. Long, C. Shao, Y. Cheng, J. Tao, X. Liu, *Applied Physics Letters* **2021**, *118*, 26 263502.

[40] V. Romero-García, N. Jiménez, J.-P. Groby, A. Merkel, V. Tournat, G. Theocharis, O. Richoux, V. Pagneux, *Phys. Rev. Applied* **2020**, *14* 054055.

[41] H. Tian, X. Xiang, K. He, C. Liu, S. Hou, S. Wang, Y. Huang, X. Wu, W. Wen, *Advanced Materials Technologies* **2021**, *6*, 12 2100668.

[42] R. Dong, D. Mao, X. Wang, Y. Li, *Phys. Rev. Applied* **2021**, *15* 024044.

[43] J. Boulvert, T. Humbert, V. Romero-García, G. Gabard, E. R. Fotsing, A. Ross, J. Mardjono, J.-P. Groby, *Journal of Sound and Vibration* **2022**, *523* 116687.

[44] J. Boulvert, G. Gabard, V. Romero-García, J.-P. Groby, *Scientific Reports* **2022**, *12*, 1 1.

[45] L. E. Kinsler, A. R. Frey, A. B. Coppens, J. V. Sanders, *Fundamentals of acoustics*, John wiley & sons, **2000**.

[46] Matlab optimization toolbox, **2019a**, The MathWorks, Natick, MA, USA.

[47] H. Bodén, M. Åbom, *The Journal of the Acoustical Society of America* **1986**, *79*, 2 541.